Progressive failure analysis and burst mode study of Type *IV* composite vessels

Shan Jin[a], Peng Cheng[a], Yong Bai[a,b,*], Jeom Kee Paik[c,d,e,f], Jun Li[b]

[a]*Architectural and Civil Engineering Department, Zhejiang University, Hangzhou 310058, P.R. China*
[b]*OPR Offshore Engineering Inc., Guangdong 510000, P.R. China*
[c]*School of Maritime and Transportation, Ningbo University, Ningbo 315000 , P.R. China*
[d]*Yantai Research Institute, Harbin Engineering University, Yantai 265615, P.R. China*
[e]*Department of Mechanical Engineering, University College London, London WC1E7JE, UK*
[f]*Lloyd's Register Foundation Research Centre of Excellence, Busan 4b241, R. Korea*

Abstract

The lightweight high pressure hydrogen storage vessels composed of polymer liner and composite reinforced layers have attracted more and more attention. In this research, a 2D axisymmetric finite element model was proposed to predict the damage evolution, failure strength and failure mode of the composite overwrapped pressure vessels, in which a user subroutine UMAT based on Hashin failure criteria was introduced to simulate the progressive damage properties of the composite material. The FE models are validated by comparison with the experimental results, and the error between the numerical simulation results and the experimental results were within 10%. It is found that vessels with different lay-up schemes might burst in different locations. Parametric studies are performed to obtain a critical ratio of hoop and helical layers to keep the vessel burst in safe mode.

Keywords: Composite material, Filament winding, Pressure vessel, Burst pressure

1. Introduction

In the present world, the global warming brought by the increased emission of greenhouse gasses into the atmosphere as a result of burning fossil fuels lead to an urgent demand for alternative sustainable clean energy. The hydrogen energy, due to its cleanness, high-efficiency, and fertile source, is becoming an increasingly practical option. [1] Yet, there are still many problems in the use of hydrogen, among which the prominent one is the transport and storage. For now, the most matured storage media is the high pressure vessel. In order to realize the need of light weight, the Type *IV* storage vessel made of a polymer liner, metal bosses, and reinforced composite layers has become one ideal choice.While the composite filament wound technology promotes the flexibility in design and manufacture, the structure of the vessel becomes complex and various design factors can significantly influence the mechanical properties of pressure vessels. [2]

Some researchers conducted burst tests to study the mechanical properties of pressure vessels and provided valuable experimental data. Wang et al. [3] investigated the relationship between acoustic emission signal characteristics and damage behaviors (matrix cracking, fiber breakage, fiber/matrix debonding) of pressure vessels during hydrostatic burst tests. The burst pressure and fracture behaviors of composite vessels were obtained by acoustic and optical sensors on the vessel specimen. Kim et al. [4] evaluated the burst pressure of vessels with a ring specimen rather than a full-scale vessel. They redesigned a ring burst test device to improve the pressure uniformity of the ring specimens. The strain variation and fracture behavior of ring specimens were evaluated by the digital image correlation method during the burst test. It should be noted that burst tests of composite pressure vessels need exorbitant time and economic costs. Therefore, the finite element analysis method has been an effective tool to conduct the burst pressure prediction and the progressive failure analysis. Over the past decades, many researchers have focused on building numerical models to optimize composite layers to improve the burst pressure of the pressure vessel and to reduce the amount of composite material. Onder et al. [5] have conducted experimental and theoretical studies to analyze the ultimate strength of composite vessels under internal pressure and obtained the optimum winding angle of composite layers. Xu et al. [6] established a 3D parametric finite element model considering different failure criteria to simulate the failure and damage evolution behavior of pressure vessels. In these studies, however, researchers only considered the cylindrical section, and neglected the influence of the dome section. These preliminary stress analyses could not accurately predict the burst pressure or burst locations of composite pressure vessels. In order to better study the mechanical behavior of composite pressure vessels, it is necessary to consider the mechanical responses of the whole pressure vessel. Various failure criteria, such as Maximum stress and strain criterion, Tsai and Wu, Hashin and Rottem, Hashin, Puck etc. [7–10], and related damage evolution laws were used in the progressive failure analysis of composite pressure vessels. Ramirez et al. [11, 12] developed a damage model exactly for the wound composite materials in the pressure vessel and validated it by a serious of tests. Incorporating this developed damage model into

*Corresponding author
Email address: baiyong@zju.edu.cn (Yong Bai)

commercial FE model, the burst test was simulated using 3D and axisymmetric elements in order to compare the advantages of these two FE models. [13] They found that both models provided almost identical results while the axisymmetric one was less computational time consuming. Liao et al. [14] applied 3D Hashin criteria and strain-based damage evolution laws to study mechanical responses and damage mechanisms of a Type *III* composite vessel. Lin et al. [15] proposed a meso-macro finite element progressive damage model based on the Puck failure criterion. They used representative volume elements (RVEs) to obtain damage variables to be fed into the macroscopic finite element models. The results showed that matrix cracking delamination occurred firstly and are finally expanded to fiber breakage with the increase of internal pressure. Jebeli et al. [16] performed a progressive damage analysis of a Type *IV* composite pressure vessel with consideration of the debonding between the composite and liner layer, and the results showed that the initial debonding did not influence the progressive damage behavior of the composite layer at the cylindrical section. Besides the prediction of the burst pressure, the burst location should also be specified precisely. As proposed in many studies, as the internal pressure of vessels increases, there may appear two kinds of burst mode, namely, safe mode (burst in the cylindrical section) and unsafe mode (burst in the dome section with the ejection of bosses). However, few researchers focused on the detailed failure mechanisms of these two burst modes.

The purpose of this paper is to study the detailed damage evolution process of different burst modes and to find the condition that the unsafe mode can be avoided. A progressive failure modeling using the axisymmetric elements is proposed. In order to simulate the damage behavior of the composite material, a UMAT subroutine is applied to introduce the stress-based Hashin-Rottem criterion and sudden degradation evolution law. The simulation results are validated by comparison with experiments. It is proved that the finite element models can well predict the burst pressure and the failure location. Finally, the evolution process of the matrix damage and fiber damage with increasing of internal pressure is presented here to discuss the mechanism of different burst modes. With the help of the validated FE model, a parametric study was carried out to find out the influence of the ratio between hoop and helical composite layers.

2. Theoretical models

2.1. Geometry model

A Type *IV* composite wound pressure vessel is composed of a polymer liner, two metallic bosses and composite reinforcement layers. The bosses are in intimate contact with the liner to keep the tightness of the whole structure. Fig. 1 shows the geometric schematization of the vessel simulated in this paper. The inner volume is 8L. The outer radius of the liner is 80 mm, the length of the cylindrical section is 424 mm, and the length of the dome, which is defined as the distance between the cylinder/dome tangent line and the polar hole, is 38 mm.

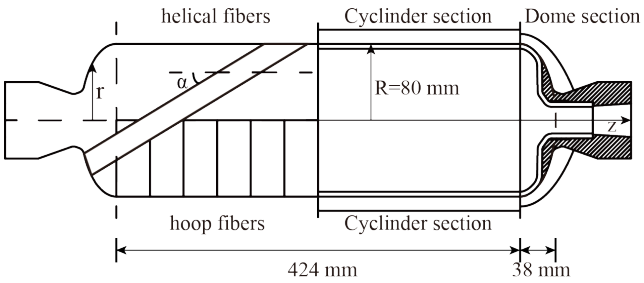

Figure 1: Geometric dimensions of the vessel.

The composite layers include two kinds of winding filaments, hoop and helical layers. There are hoop and helical layers at the cylindrical part and only helical layers at the dome section. The hoop layers are wound with an angle close to 90 degree.

In this paper, the helical filament is considered following a geodesic path, which presents the shortest distance between any two points on the surface. The angle α denotes the winding angle of the helical filament, whereas α_0 locates at the cylindrical section. on the surface of revolution, the geodesic path is defined by Clairaut's equation:

$$r \sin \alpha = const \tag{1}$$

Noting that the filament is tangent to the boss at the polar hole, resulting in a winding angle of 90 degree, the Eq. 1 can be changed as following:

$$\sin \alpha = \frac{r_0}{r} \tag{2}$$

where r_0 is the radius of the polar hole.

After the winding angle is determined, the thickness distribution of the filament at the dome is defined as:

$$t(r) = \frac{t_p \cos \alpha_0}{\cos \alpha} \times \frac{R}{r + 2b(\frac{R-r}{R-r_0})^4} \tag{3}$$

where t_p is the thickness in the cylinder section, r is the current radius and b is the helical band width. This last parameter in this equation controls the thickness growth at the turnaround point.

2.2. Elastic moduli of the fiber composite

The vessel discussed in this paper is overwrapped by glass fiber/epoxy composites. A simplification of the section of the composite lamina is shown in Fig. 2. The composite is consisted of matrix and unidirectionally oriented fibers. The material coordinate system is defined as that 1 denotes the longitudinal direction along the fiber, 2 denotes the transverse direction, 3 denotes the through-thickness direction. It is usually assumed that a unidirectional fiber-reinforced composite can be treated as transversely isotropic, that is $E_2 = E_3$, $G_{12} = G_{13}$, $\nu_{12} = \nu_{13}$ and $G_{23} = E_2/2(1+\nu_{23})$. The properties of the composite can be analytically predicted from those of the constituent properties. There are several different methods available in the literature's

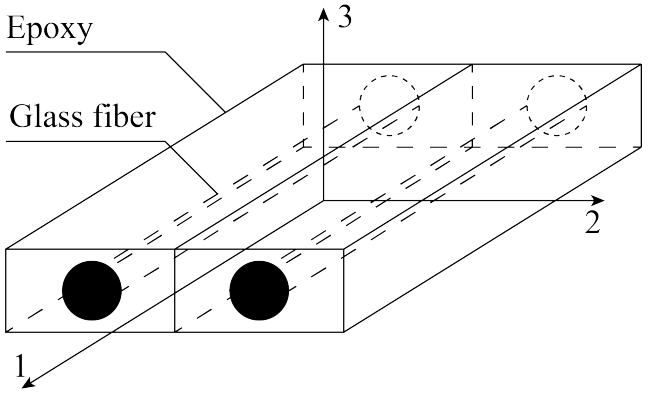

Figure 2: Simplification of the composite lamina.

Table 1: Determination of composite properties from fiber and matrix properties

Elastic constant	P	P_f	P_m	η
E_1	E_1	E_{1f}	E_m	1
ν_{12}	ν_{12}	ν_{12f}	ν_m	1
G_{12}	$1/G_{12}$	$1/G_{12f}$	$1/G_m$	η_6
G_{23}	$1/G_{23}$	$1/G_{23f}$	$1/G_m$	η_4
K_T	$1/K_T$	$1/K_f$	$1/K_m$	η_K

[9, 17–19]. Among these, the material model proposed by Hahn [9] can obtain relatively true results through a set of simple calculations and is utilized in this paper. Hahn's model states that the elastic properties of composite, fiber and matrix have the following functional form:

$$P = \frac{P_f V_f + \eta P_m V_m}{V_f + \eta V_m} \tag{4}$$

where V_f and V_m are the volume fractions of the fibers and matrix, respectively and definition of each group of elastic constant P, P_f, P_m and η are given in Table 1.

Here, K_f and K_m are the plane strain bulk modulus of fiber and matrix, respectively. For isotropic material such as glass fiber, K equals to $G/(1-2\nu)$. In the Table 1, the η are calculated as follow:

$$\begin{aligned} \eta_6 &= \frac{1 + G_m/G_{12f}}{2} \\ \eta_4 &= \frac{3 - 4\nu_m + G_m/G_{23f}}{4(1-\nu_m)} \\ \eta_K &= \frac{1 + G_m/K_f}{2(1-\nu_m)} = \frac{1 + (1-2\nu_f)G_m/G_f}{2(1-\nu_m)} \end{aligned} \tag{5}$$

The transverse moduli of the composite are calculated by the following equation:

$$E_2 = E_3 = \frac{4K_T G_{12}}{K_T + mG_12} \tag{6}$$

where

$$m = 1 + \frac{4K_T \nu_{12}^2}{E_1} \tag{7}$$

Finally, the the Poisson's ratio, ν_{23}, can be calculated by the Equation.

$$\nu_{23} = \nu_f V_f + \nu_m (1 - V_f) \frac{1 + \nu_m - \nu_{12}(E_m/E_1)}{1 - \nu_m^2 + \nu_m \nu_{12}(E_m/E_1)} \tag{8}$$

3. Progressive failure analysis

3.1. Finite element modeling

The composite wound vessel simulated in this papert is composed of a polymer liner, 6061-T6 aluminum bosses and composite reinforced layers. Due to the high strength of the composite layers, the polymer liner only has small deformation before burst happens. Therefore, the polymer material is treated as elastic material. The plastic property is considered for the aluminum and the elastic-perfectly plasticity model is used. The mechanical properties of these two material are shown in Table. 2. The glass fiber/matrix composite can be treated as a brittle material, which suffers brittle breakage without plastic deformation. Therefore the plastic properties of the composite are neglected in this paper, and the elastic material properties are summarized in the Table. 3.

Due to the rotationally symmetric structure of hydrogen storage vessel, a 2D axisymmetric finite element model generated by ABAQUS software was made in this paper. According to the available literature [13], this kind of model provides an identical result to that of the 3D model, as well as consumes much less computational time. In the model generation process, the liner and polar bosses are made firstly. Once these parts have been generated, the wound composite layers can be defined to overwrap the inner structures. As shown in Fig. 3, the red line represents the outline over which filament wound layers will be laid. In this paper, the Wound Composite Modeler (WCM) plug-in is used to generate the wound compoiste layers. with the help of WCM plug-in, a series of parameters such as layer thickness, wind angle, layer material properties can be specified for each composite layer to simulate the actual vessel specimen. Finally, the different parts of the tank are put together, assuming a perfect junction between each other by assigning tie connections to the interaction surface. The resultant model is illustrated in Fig. 3. The 2D axisymmetric model is placed at the $O - XY$ plane, with the Y-axis as the rotation axis. In the generation process, each composite layer is assigned a local coordinate system. The coordinate system is shown in Fig. 4, where x denotes the meridian direction, y denotes the through thickness direction and z denotes the hoop direction. It should be noted that It should be noted that quantities directly obtained from Abaqus are along the local coordinate system, $o - xyz$.

Table 2: Mechanical properties of polymer PA6 and aluminum 6061-T6

PA6		6061-t6		
E(MPa)	ν	E(MPa)	ν	σ_s(MPa)
1880	0.28	74120	0.4	47

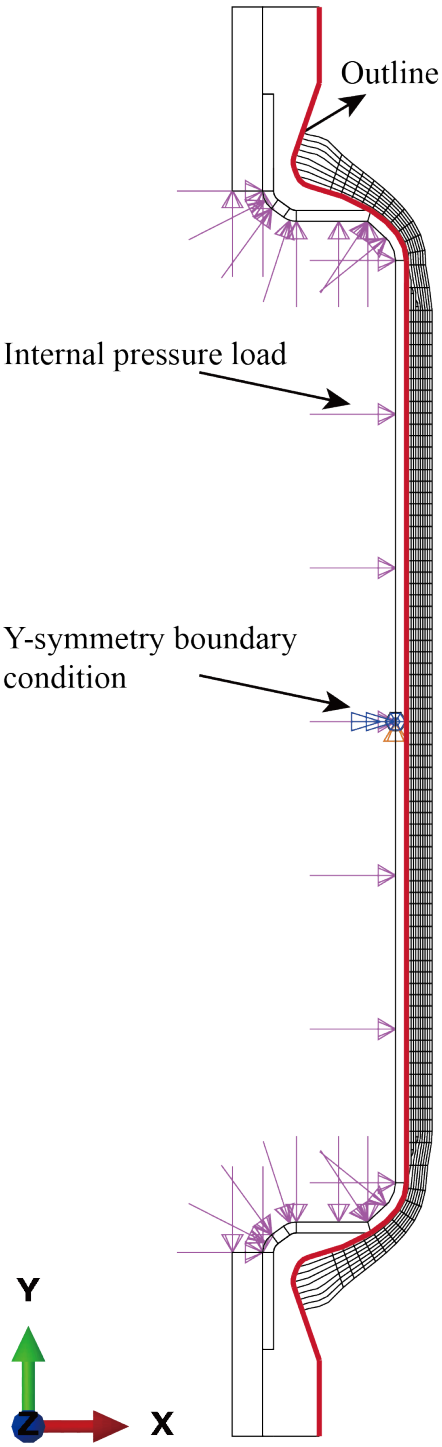

Figure 3: Mesh and boundary conditions of the finite element model.

Table 3: Mechanical properties of composite

Longitudinal modulus, E_1 (MPa)	45600
Tranverse modulus, E_2 (MPa)	10680
Through-thickness modulus, E_3 (MPa)	10680
In-plane shear modulus, G_{12} (Mpa)	4250
Transverse shear modulus, G_{13} (MPa)	4250
Through-thickness shear modulus, G_{23} (MPa)	3700
Major Poisson's ratio, ν_{12}	0.26
Major Transverse Poisson's ratio, ν_{13}	0.26
Through-thickness Poisson's ratio, ν_{23}	0.33
longitudinal tensile strength, X_t (Mpa)	860
longitudinal compressive strength, X_c (MPa)	517
Transverse tensile strength, Y_t (MPa)	40
Transverse compressive strength,Y_c (MPa)	145
Longitudinal shear strength, S (MPa)	73

3.2. *Transformation of the constitutive relation*

In the material coordinates, $o-123$, the constitutive relation can be written as follows:

$$\begin{Bmatrix}\sigma_1\\ \sigma_2\\ \sigma_3\\ \sigma_{12}\\ \sigma_{13}\\ \sigma_{23}\end{Bmatrix} = \begin{bmatrix}C_{11} & C_{12} & C_{13} & 0 & 0 & 0\\ C_{21} & C_{22} & C_{23} & 0 & 0 & 0\\ C_{31} & C_{32} & C_{33} & 0 & 0 & 0\\ 0 & 0 & 0 & C_{44} & 0 & 0\\ 0 & 0 & 0 & 0 & C_{55} & 0\\ 0 & 0 & 0 & 0 & 0 & C_{66}\end{bmatrix}\begin{Bmatrix}\epsilon_1\\ \epsilon_2\\ \epsilon_3\\ \gamma_{12}\\ \gamma_{13}\\ \gamma_{23}\end{Bmatrix} \tag{9}$$

$$\begin{aligned}
C_{11} &= E_1(1-\nu_{23}\nu_{32})/\Lambda\\
C_{22} &= E_2(1-\nu_{13}\nu_{31})/\Lambda\\
C_{33} &= E_3(1-\nu_{12}\nu_{21})/\Lambda\\
C_{12} &= C_{21} = E_1(\nu_{21}+\nu_{31}\nu_{23})/\Lambda\\
C_{13} &= C_{31} = E_1(\nu_{31}+\nu_{21}\nu_{32})/\Lambda\\
C_{23} &= C_{32} = E_2(\nu_{32}+\nu_{12}\nu_{31})/\Lambda\\
C_{44} &= G_{12}\\
C_{55} &= G_{13}\\
C_{66} &= G_{23}\\
\Lambda &= 1-\nu_{12}\nu_{21}-\nu_{13}\nu_{31}-\nu_{23}\nu_{32}-2\nu_{12}\nu_{21}\nu_{32}
\end{aligned} \tag{10}$$

where E_i are the Young's modulus, ν_{ij} are the Poisson ratio and G_{ij} are the shear modulus. It should be noted that the shear strains used in this paper are engineering shear strains.

The stress tensor between local coordinates and material coordinates can be transformed by the following relations:

$$\begin{bmatrix}\sigma_{11} & \sigma_{12} & \sigma_{13}\\ \sigma_{21} & \sigma_{22} & \sigma_{23}\\ \sigma_{31} & \sigma_{32} & \sigma_{33}\end{bmatrix} = \begin{bmatrix}l_1 & m_1 & n_1\\ l_2 & m_2 & n_2\\ l_3 & m_3 & n_3\end{bmatrix}\begin{bmatrix}\sigma_{xx} & \sigma_{xy} & \sigma_{xz}\\ \sigma_{yx} & \sigma_{yy} & \sigma_{yz}\\ \sigma_{zx} & \sigma_{zy} & \sigma_{zz}\end{bmatrix}\begin{bmatrix}l_1 & l_2 & l_3\\ m_1 & m_2 & m_3\\ n_1 & n_2 & n_3\end{bmatrix} \tag{11}$$

where l_i, m_i and n_i are direction cosines between different coordinate axes, which are shown in 4. where l_i, m_i and n_i are direction cosines between different coordinate axes, which are

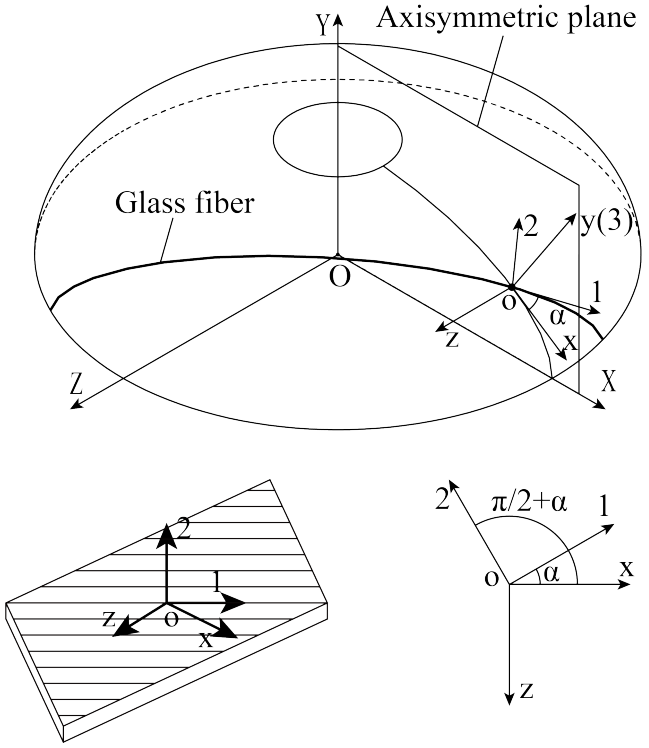

Figure 4: A schematic of different coordinate systems.

Table 4: Direction cosines between different coordinates

	x	y	z
1	l_1	m_1	n_1
2	l_2	m_2	n_2
3	l_3	m_3	n_3

	x	y	z
1	$\cos\alpha$	0	$-\sin\alpha$
2	$-\sin\alpha$	0	$-\cos\alpha$
3	0	1	0

shown in the Table 4. The transformation matrices for strain tensor and stress tensor are the same. However, it should be noted that the shear strain directly obtained from the ABAQUS is engineering strain, γ_{ij}, which is equal to two times of tensor stain, ϵ_{ij}. Therefore, the stress and strain transformation matrices are different, and are defined by the following:

$$\boldsymbol{T_\sigma} = \begin{bmatrix} C^2 & 0 & S^2 & 0 & -2SC & 0 \\ S^2 & 0 & C^2 & 0 & 2SC & 0 \\ 0 & 1 & 0 & 0 & 0 & 0 \\ -SC & 0 & SC & 0 & S^2 - C^2 & 0 \\ 0 & 0 & 0 & C & 0 & -S \\ 0 & 0 & 0 & -S & 0 & -C \end{bmatrix} \tag{12}$$

$$\boldsymbol{T_\epsilon} = \begin{bmatrix} C^2 & 0 & S^2 & 0 & -SC & 0 \\ S^2 & 0 & C^2 & 0 & SC & 0 \\ 0 & 1 & 0 & 0 & 0 & 0 \\ -2SC & 0 & 2SC & 0 & S^2 - C^2 & 0 \\ 0 & 0 & 0 & C & 0 & -S \\ 0 & 0 & 0 & -S & 0 & -C \end{bmatrix} \tag{13}$$

where $S = \sin\alpha$ and $C = \cos\alpha$ The stiffness matrix in the local coordinate system, $\overline{\boldsymbol{C}}$, can be transformed from the stiffness matrix in the material coordinate system, $\boldsymbol{C}$ as following:

$$\overline{\boldsymbol{C}} = \boldsymbol{T_\sigma^{-1}} \boldsymbol{C} \boldsymbol{T_\epsilon} \tag{14}$$

It should be noted that $\overline{\boldsymbol{C}}$ is a 6×6 matrix, which can not be used directly in the axisymmetric model presented in this paper. A new 4×4 matrix, $\overline{\boldsymbol{C}}'$ should be calculated:

$$\overline{\boldsymbol{C}}' = \boldsymbol{q} \overline{\boldsymbol{C}} \boldsymbol{q}^T \tag{15}$$

where

$$\boldsymbol{q} = \begin{bmatrix} 1 & 0 & 0 & 0 & 0 & 0 \\ 0 & 1 & 0 & 0 & 0 & 0 \\ 0 & 0 & 1 & 0 & 0 & 0 \\ 0 & 0 & 0 & 1 & 0 & 0 \end{bmatrix} \tag{16}$$

3.3. Damage model

In order to analysis the mechanical behavior of pressure vessels and predict the burst pressure, it is necessary to introduce the progressive damage model to simulate the failure behavior of composite materials. In this study, the progressive failure is initiated as soon as the element satisfies the Hashin-Rottem criterion, which are defined as follows:

$$\begin{aligned} &\text{tensile fiber failure, } \sigma_1 > 0 \\ &F_f = (\frac{\sigma_1}{X_T})^2 \le 1 \\ &\text{compressive fiber failure, } \sigma_1 \le 0 \\ &F_f = (\frac{\sigma_{11}}{X_C})^2 \le 1 \\ &\text{tensile matrix failure, } \sigma_2 + \sigma_3 > 0 \\ &F_m = (\frac{\sigma_2}{Y_T})^2 + (\frac{\tau_{12}}{S})^2 \le 1 \\ &\text{compressive matrix failure, } \sigma_2 + \sigma_3 \le 0 \\ &F_m = (\frac{\sigma_2}{Y_C})^2 + (\frac{\tau_{12}}{S})^2 \le 1 \end{aligned} \tag{17}$$

where subscripts X, Y and S express longitudinal, transverse and shear strength of composite, and T and C are longitudinal and transverse directions, respectively.

Once the stress field of one element reaches these criterion, the failure behavior will be taken into account by degrading the initial stiffness matrix to characterize the damaged material. Elements of the degraded stiffness matrix, $\boldsymbol{C_d}$ are expressed as follows:

$$\begin{aligned} CD_{11} &= (1 - d_f) * C_{11} \\ CD_{12} &= CD_{21} = (1 - d_f) * (1 - d_m) * C_{12} \\ CD_{13} &= CD_{31} = (1 - d_f) * C_{13} \\ CD_{22} &= (1 - d_m) * C_{22} \\ CD_{23} &= CD_{32} = (1 - d_m) * C_{23} \\ CD_{44} &= (1 - d_f) * (1 - d_m) * C_{44} \\ CD_{ij} &= C_{ij} \text{ for other items.} \end{aligned} \tag{18}$$

One UMAT subroutine written by FORTRAN code is introduced to implement this discrimination process. At every increment step, this subroutine was used to transform the strain and

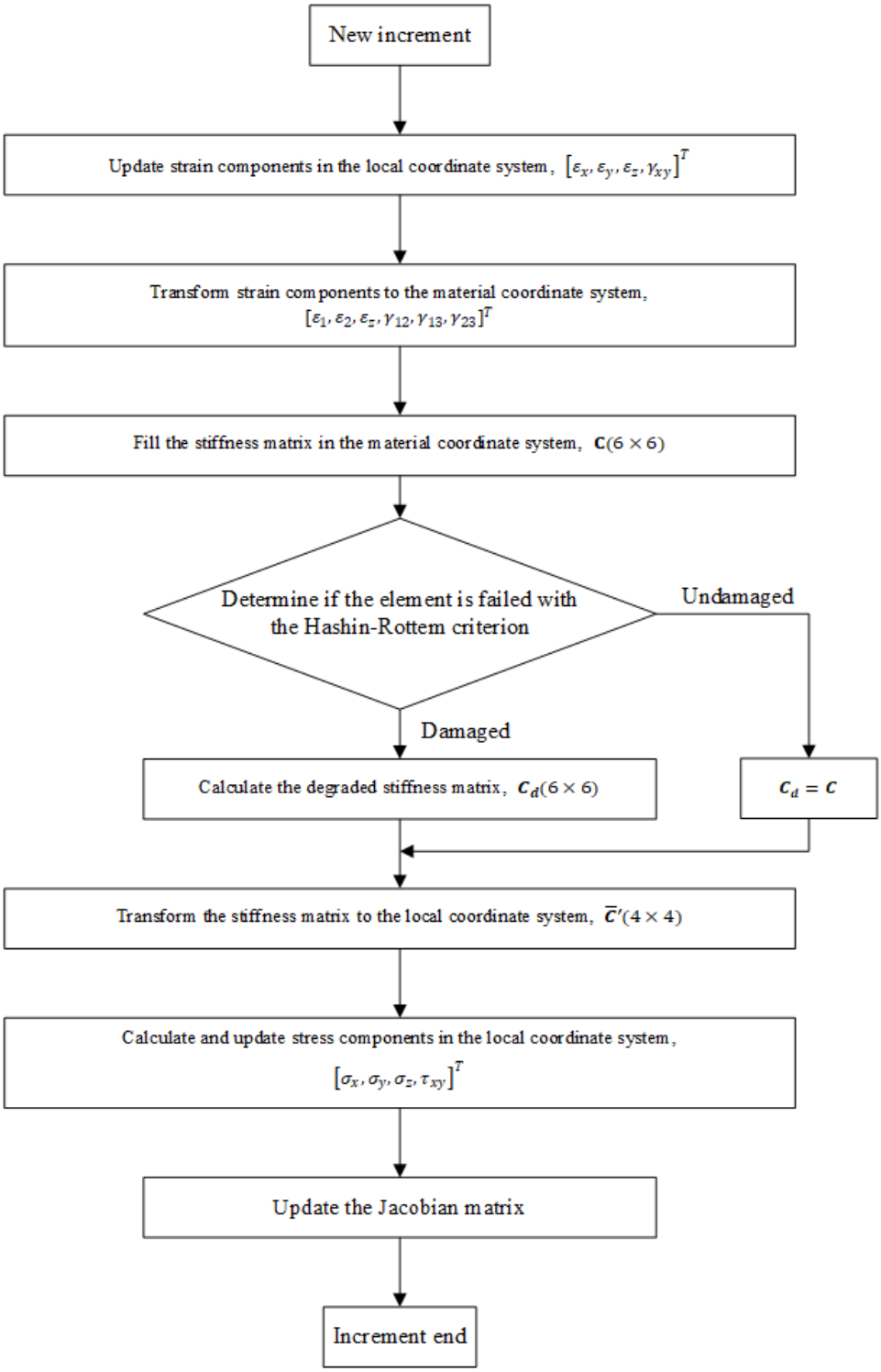

Figure 5: A schematic of different coordinate systems. Directions 1, 2 and 3 coincide with tangent, through-thickness and hoop directions; Directions 1‘, 2‘ and 3‘ coincide with fiber, transverse and through-thickness directions.

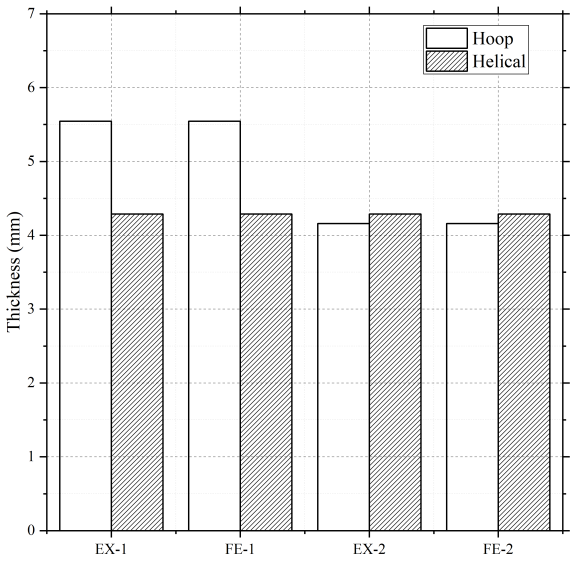

Figure 6: Thickness distribution of composite layers of experimental specimens and corresponding models.

ID	FE-A	EX-A	EX-B	FE-B
	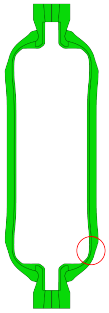			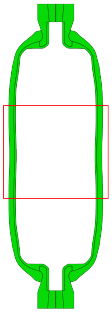
Mode	Unsafe	Unsafe	Safe	Safe
Pressure	63.00	65.20	65.17	62.00
Error	3.4%	—	—	4.9%

Figure 7: Results of the experiments and FE simulations.

stress between different coordinate systems as well as decide if the element fails. The detailed analysis procedure is shown in Fig. 5.

4. Simulation of the mechanical behavior of the tank under internal pressure

4.1. Validation of the FE model

In order to validate the finite element model presented in this paper, two composite overwrapped pressure vessels, with the label of EX-A and EX-B, were designed and tested to burst. Numerical models were built by the procedure mentioned above to simulate the experimental results. The thickness distribution of hoop and helical layers are shown in Fig.6. It can be found that there were the same helical composite layers in these two specimens, whereas more hoop layers were wound for the EX-A. Collapse pressures as well as burst modes of two experiments are listed in Fig.7. As shown in the figure, two different burst modes were found in the tests, namely unsafe mode and safe mode. For the EX-A, burst occurred in the dome section with the ejection of one metallic boss. This failure mode is thought as the unsafe mode, because the ejection of the boss will lead to serve consequence in the actual situation. The EX-B exploded at the cylinder section and the vessel still maintained one whole part. This kind of failure mode is thought as the safe burst mode. It should be noted that burst pressures of these two cases were nearly the same. This result proves that when vessels burst in the unsafe mode, overuse of hoop layers will not increase the internal pressure carrying capacity of the vessel. Simulation results of the finite element models were also summarized in Fig.7. The burst locations predicted by the FE model compared well with the experiments. Comparing the actual burst pressure and numerical simulation pressure, the maximum error of prediction is 4.9% and the simulated bursting pressures were lower than the experimental bursting pressures. This result denotes that the finite element model is capable of predicting the burst pressure and burst mode.

4.2. Discussions on the different bursting modes

Based on the previous validation result, detailed analysis of the mechanical behaviors of composite pressure vessels failed in different burst modes will be done with the simulating results. The FE-A predicted an unsafe burst mode. The displacement versus inner pressure curves are shown in Fig.8(a) and the damage distribution contours at different inner pressures are shown in Fig.8(b). In Fig.8(a), the left horizontal axis presents the radial displacement at the tangent line of the liner, U1 and the right horizontal axis is the axial displacement at the top of the metal boss, U2. These diagrams give valuable information to research the failure mechanism for the pressure vessel in both global and local damage perspectives. As shown by these graphs, there are several key points which divide the curves into distinct regions. The first linear part denotes the initial elastic behavior of the whole structure. The matrix damage firstly appears at the internal pressure of 43 MPa, and it is mainly located at the inner portion of the helical winding layers in the dome section. The occurrence of matrix damage has little effect on the trend of curves. With the increase of internal pressure, the matrix damage propagated only in the dome section until the fiber damage appears in the dome section for the first time at 55 MPa. Between 55 MPa and 63 MPa, the matrix damage spreads through the dome section and the fiber damage propagates from the inside to the outside. The displacement curves raise faster, indicating a decline of the strength of the structure. Finally, at 63 MPa, a penetrating fiber damage zone is formed at the done section. The vessel is thought to be exploded at this location which is consistent with the experiment result. In the finite element simulation, large deformation will concentrate at this location in the post burst region. During the whole loading process, no fiber damage appears to the cylinder of the vessel. This phenomenon indicates that when the vessel burst in the un-

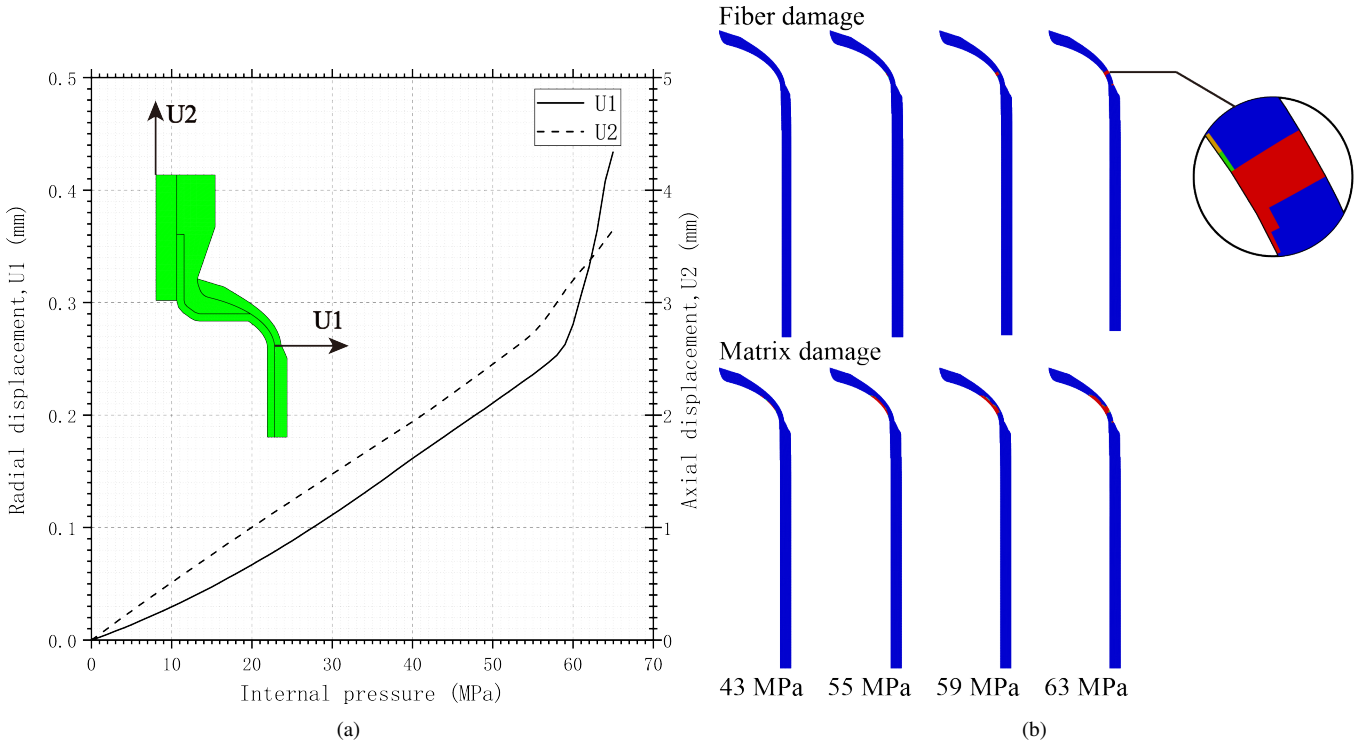

Figure 8: (a) Displacement versus internal pressure curves; (b) fiber damage and matrix damage at different internal pressures for the finite element model, FE-A.

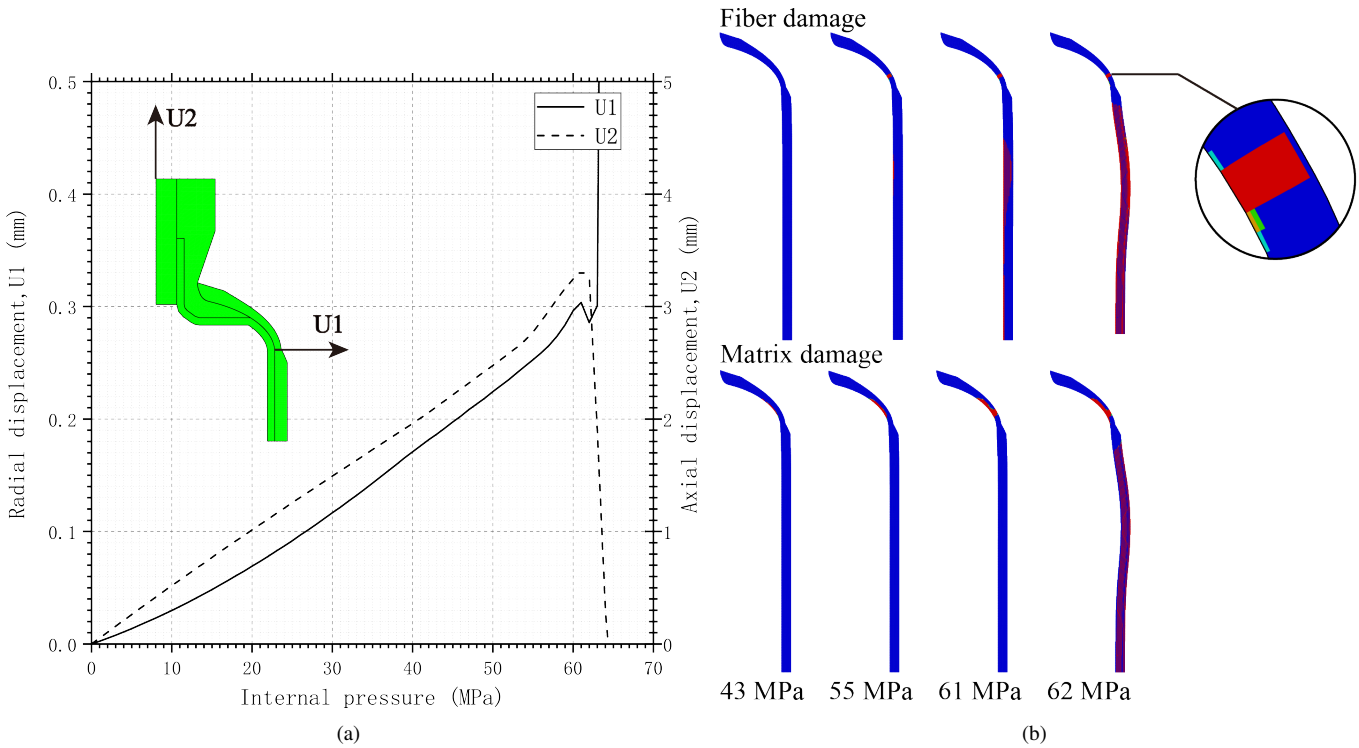

Figure 9: (a) Displacement versus internal pressure curves; (b) fiber damage and matrix damage at different internal pressures for the finite element model, FE-B.

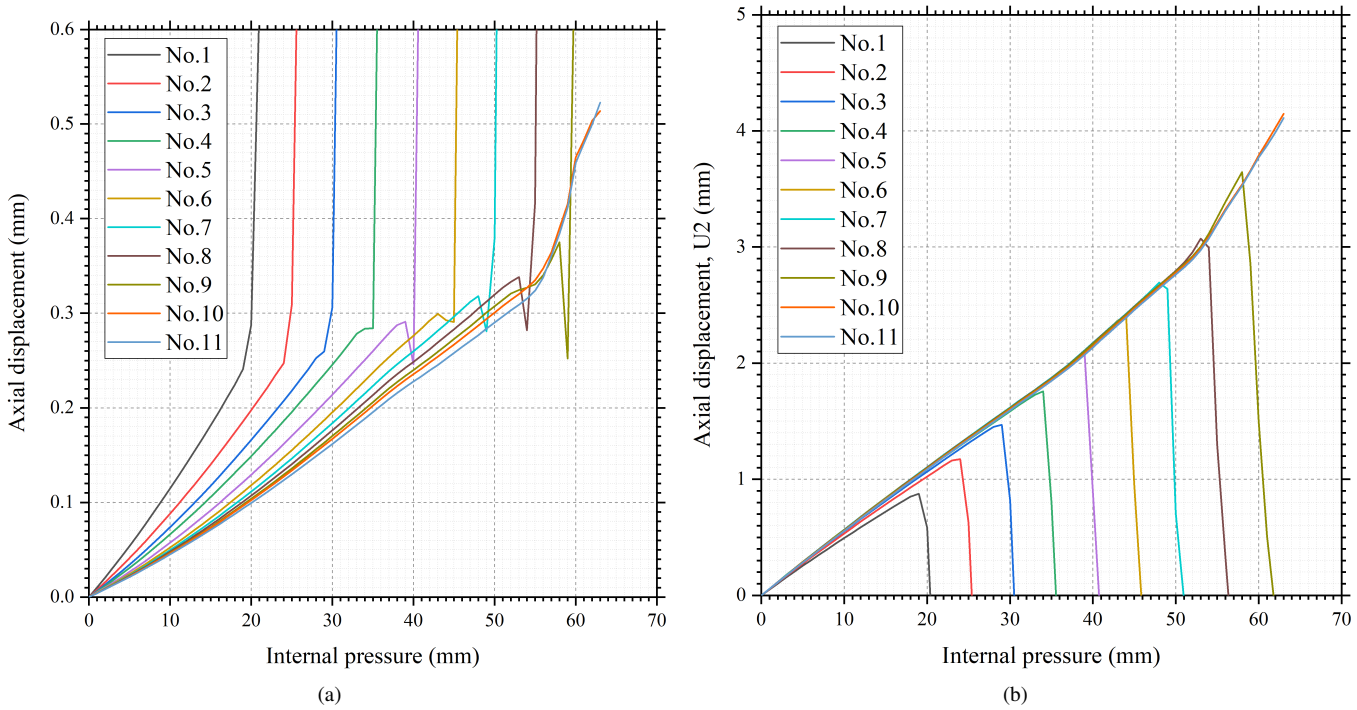

Figure 10: (a) Axial displacement versus internal pressure curves; (b) radial displacement at the tangent line versus internal pressure curves for finite element models.

safe mode, the strength of the reinforced composites is not fully utilized.

Another model, FE-B predicted a safe burst mode. Similarly, the displacement curves and damage distribution contours are shown in Fig.9. At the pressure of 43 MPa, the matrix damage appears at the helical layers in the dome section for the first time, which did not have any effect on the displacement curves. When the pressure increased to 55 MPa, the fibre damage occurred at the dome portion and the matrix damage continued to spread. The displacement curves increased faster until the hoop layers in the cylinder section sustained fiber damage firstly at 61 MPa. With increasing pressure, the redistribution of stress made the fibre damage spread rapidly from the inside to the exterior. At 62 MPa, all the hoop layers broke and the structure lost the bearing capacity. Meanwhile, the fracture of hoop composite also lead to the occurrence of matrix damage at the helical composite in the cylinder section. As a consequence, the axial displacement of the hydrogen storage vessel suddenly dropped, whereas the radial displacement had an enormous growth. It should be noted in this case that, the helical layers in the dome section also sustained fiber damage, which developed from the inner layer to the outside. However, breakage occurred earlier at the cylinder section before a penetrating fiber damage zone was formed. The simulation result indicates the burst position occurs at the cylinder section of the hydrogen storage vessel and the metal boss will not be ejected. Therefore, this case is thought as a safe mode.

4.3. Threshold thickness ratio to ensure safe burst mode of vessels

As shown in the above discussion, the mechanical behaviors of vessels are related to the composite lay-up. This section aims to carry out a parametric study on the effect of the ratio of hoop to helical layers on the mechanical behaviors and burst modes of pressure vessels. In this section, the ratio thickness of hoop layers to that of helical layers is defined as the composite thickness ratio, γ. Eleven finite element models in total were built to carry out a detailed investigation on the mechanical behaviors of vessels with various values of γ. The thickness distributions of these models are summarized in the Table.5. The thickness of helical composite layers of all the models is the same while the hoop composite thickness varies to make different values of γ.

Fig.10 shows the displacements versus internal pressure curves for every model. Meanwhile, burst pressures and burst modes are summarized in the Fig. 11. At first, the ultimate burst pressure increases linearly with increasing γ and models are predicted to burst in the safe mode. The fiber damage started to occur at the helical layers in the dome section from the No.8. It can be found from the displacement graphs that the curves increase faster at one pressure due to the decline of strength of helical composite in dome section. However, the model still burst in the cylinder portion. Further increase in γ leads to a plateau in burst pressure. The value of γ at the turning point is defined as the threshold thickness ratio, γ_{th}. When the ratio is larger than this value, the model will burst in the dome section.

On the basis of distribution of fiber damage when the vessel burst, the failure of the vessel can be classified into three situ-

Table 5: Thickness distribution of composite layers of finite element models

No.	1	2	3	4	5	6	7	8	9	10	11
t_{hoop} (mm)	0.5	1.0	1.5	2.0	2.5	3.0	3.5	4.0	4.5	5.0	5.5
$t_{helical}$ (mm)	4.0	4.0	4.0	4.0	4.0	4.0	4.0	4.0	4.0	4.0	4.0
composite thickness ratio, γ	0.125	0.25	0.375	0.5	0.625	0.75	0.875	1	1.125	1.25	1.375

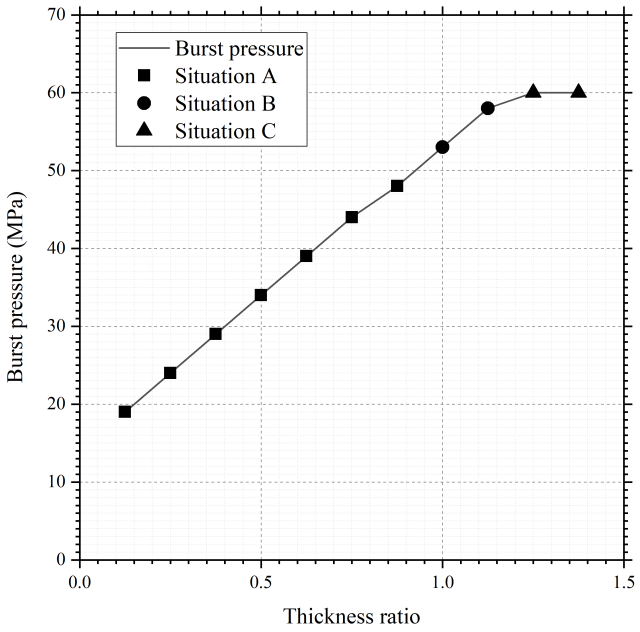

Figure 11: Simulation results of parametric models.

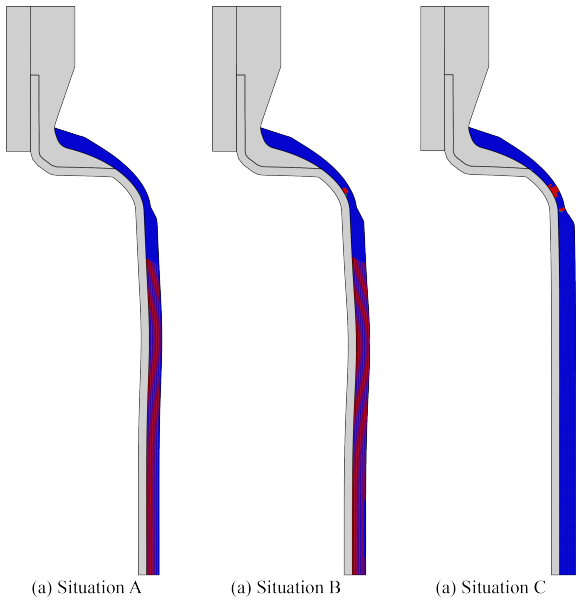

Figure 12: Distribution of fiber damage for different situations.

ations as shown in the figure. The situation A happens for the first seven models with small γ. In this situation, the fiber damage only occurs at the hoop composite layers in the cylindrical portion and the vessel will explode when all the hoop fibers break. During the loading process, there is no fiber damage at the helical composite layers. Therefore, this region of γ can fully ensure that the vessel bursts in the safe mode.

The situation B happens for the models, No. 8 and No. 9, of which the composite ratio is near to γ_{th}. It can be found that when the ultimate strength is reached, the fiber damage occurs at both dome and cylindrical portions. However, the entire hoop layers have broke before a penetrating damage zone is formed at the helical layers in the dome section. The composite ratio of specimen used in validation experiment, EX-B, belongs to this region. Both experimental and numerical results show the vessel will burst in the safe mode. It should be noted that the strength of helical and hoop layers are fully utilized and the burst pressure is near the peak value in this parametric study. However, the damage distribution indicates the risk that vessels may burst in the dome section still exists. Therefore, designers should be careful with this region of γ in the actual manufacture process.

The situation C happens to models with γ larger than γ_{th}. The model predicted an explosion in the dome section when a penetrating fiber damage zone is formed. It is interesting to find that the overuse of hoop layers will not increase the burst pressure any more. Therefore, the composite ratio should be controlled bellow the γ_{th} to ensure the safe burst mode as well as to avoid material waste.

5. Conclusions

The aim of the present research was to examine the mechanical behavior of composite overwrapped pressure vessels under internal pressure. A progressive failure finite element model was made with 2D axisymmetric elements to carry out burst simulations. One UMAT subroutine was written to implement Hashin-Rottem damage model to the composite layers and realize a transformation algorithm. The comparison between the experimental and numerical results confirmed that the models were capable of predicting the burst pressure and burst mode. With the help of FE simulations, the mechanism of different burst modes was carefully analyzed with both global deformation and local damage development. Termination conditions for different burst modes were determined. A vessel will burst in the safe mode when the hoop layers break before a penetrating fiber damage zone is formed at the helical layers in the dome section. Otherwise, the vessel will burst in the unsafe mode when all the helical fibers in the dome section break. Another valuable finding is that when the helical layers are the same, the distribution of hoop layers will not influence the mechanical behavior in the dome section. Based on this, the dome and cylinder sections can be analyzed separately in the further theoretical

study. Mechanical behaviors of vessels with different composite thickness ratios, γ were investigated by a parametric numerical study. The threshold thickness ratio, γ_{th} is determined at which the burst mode of vessels changes from the safe mode to the unsafe mode. It was found that when the γ was larger than the γ_{th}, the burst pressure would not be increased even if more hoop layers were added. This finding is valuable in the optimal design to reduce manufacture cost and ensure safe burst mode. However, a limitation of this study is that more possible influence factors on the γ_{th} (such as geometry of the liner, material properties, winding angles, etc.) are not taken into consideration. Further work needs to be done to establish the ratio for different situations.

6. Disclosure statement

No potential conflict of interest was reported by the author(s).

References

[1] B. Pivovar, N. Rustagi, S. Satyapal, Hydrogen at scale (h2@ scale): key to a clean, economic, and sustainable energy system, The Electrochemical Society Interface 27 (1) (2018) 47.

[2] M. Azeem, H. H. Ya, M. Kumar, P. Stabla, M. Smolnicki, L. Gemi, R. Khan, T. Ahmed, Q. Ma, M. R. Sadique, et al., Application of filament winding technology in composite pressure vessels and challenges: a review, Journal of Energy Storage 49 (2022) 103468.

[3] D. Wang, B. Liao, C. Hao, A. Wen, J. Zheng, P. Jiang, C. Gu, P. Xu, Q. Huang, Acoustic emission characteristics of used 70 mpa type iv hydrogen storage tanks during hydrostatic burst tests, International Journal of Hydrogen Energy 46 (23) (2021) 12605–12614.

[4] W. T. Kim, S. S. Kim, Design of a segment-type ring burst test device to evaluate the pressure resistance performance of composite pressure vessels, Composite Structures 242 (2020) 112199.

[5] A. Onder, O. Sayman, T. Dogan, N. Tarakcioglu, Burst failure load of composite pressure vessels, Composite structures 89 (1) (2009) 159–166.

[6] P. Xu, J. Zheng, P. Liu, Finite element analysis of burst pressure of composite hydrogen storage vessels, Materials & Design 30 (7) (2009) 2295–2301.

[7] S. W. Tsai, E. M. Wu, A general theory of strength for anisotropic materials, Journal of composite materials 5 (1) (1971) 58–80.

[8] Z. Hashin, A. Rotem, A fatigue failure criterion for fiber reinforced materials, Journal of composite materials 7 (4) (1973) 448–464.

[9] H. Hahn, Simplified formulas for elastic moduli of unidirectional continuous fiber composites, Journal of Composites, Technology and Research 2 (3) (1980) 5–7.

[10] A. Puck, H. Schürmann, Failure analysis of frp laminates by means of physically based phenomenological models, in: Failure criteria in fibre-reinforced-polymer composites, Elsevier, 2004, pp. 832–876.

[11] J. P. B. Ramirez, D. Halm, J.-C. Grandidier, S. Villalonga, A fixed directions damage model for composite materials dedicated to hyperbaric type iv hydrogen storage vessel–part i: Model formulation and identification, International Journal of Hydrogen Energy 40 (38) (2015) 13165–13173.

[12] J. P. B. Ramirez, D. Halm, J.-C. Grandidier, S. Villalonga, A fixed directions damage model for composite materials dedicated to hyperbaric type iv hydrogen storage vessel–part ii: Validation on notched structures, International Journal of Hydrogen Energy 40 (38) (2015) 13174–13182.

[13] J. P. B. Ramirez, D. Halm, J.-C. Grandidier, S. Villalonga, F. Nony, 700 bar type iv high pressure hydrogen storage vessel burst–simulation and experimental validation, International Journal of Hydrogen Energy 40 (38) (2015) 13183–13192.

[14] B.-b. Liao, D.-l. Wang, L.-y. Jia, J.-y. Zheng, C.-h. Gu, Continuum damage modeling and progressive failure analysis of a type iii composite vessel by considering the effect of autofrettage, Journal of Zhejiang University-SCIENCE A 20 (1) (2019) 36–49.

[15] S. Lin, L. Yang, H. Xu, X. Jia, X. Yang, L. Zu, Progressive damage analysis for multiscale modelling of composite pressure vessels based on puck failure criterion, Composite Structures 255 (2021) 113046.

[16] M. A. Jebeli, M. Heidari-Rarani, Development of abaqus wcm plugin for progressive failure analysis of type iv composite pressure vessels based on puck failure criterion, Engineering Failure Analysis 131 (2022) 105851.

[17] J. Halpin, S. Tsai, Environmental factors in composite materials design, US Air Force Technical Report AFML TR 67423 (1967).

[18] Z. Hashin, Theory of fiber reinforced materials (1972).

[19] R. M. Christensen, Mechanics of composite materials, Courier Corporation, 2012.